11 April 2013

Report

DOE

ID: 0015332

DOE Prog. Mgr.: Dr. Renu Joseph

Award Reg.#: ER64851

Title: North Pacific Mesoscale Coupled Air-Ocean Simulations Compared with Observations

DRI Project Director/Principal Investigator: Dr. Darko Koracin

DRI Team members: Dr. Ramesh Vellore, Dr. John Mejia, Mr. Benjamin Hatchett, Mr. Travis McCord

Scripps collaborators: Dr. Ivana Cerovecki, Dr. Julie McLean, Dr. Clive Dorman

Executive summary

The main objective of the study was to investigate atmospheric and ocean interaction processes in the western Pacific and, in particular, effects of significant ocean heat loss in the Kuroshio and Kuroshio Extension regions on the lower and upper atmosphere. It is yet to be determined how significant are these processes are on climate scales. The understanding of these processes led us also to development of the methodology of coupling the Weather and Research Forecasting model with the Parallel Ocean Program model for western Pacific regional weather and climate simulations. We tested NCAR-developed research software Coupler 7 for coupling of the WRF and POP models and assessed its usability for regional-scale applications. We completed test simulations using the Coupler 7 framework, but implemented a standard WRF model code with options for both one- and two-way mode coupling. This type of coupling will allow us to seamlessly incorporate new WRF updates and versions in the future. We also performed a long-term WRF simulation (15 years) covering the entire North Pacific as well as high-resolution simulations of a case study which included extreme ocean heat losses in the Kuroshio and Kuroshio Extension regions. Since the extreme ocean heat loss occurs during winter cold air outbreaks (CAO), we simulated and analyzed a case study of a severe CAO event in January 2000 in detail. We found that the ocean heat loss induced by CAOs is amplified by additional advection from mesocyclones forming on the southern part of the Japan Sea. Large scale synoptic patterns with anomalously strong anticyclone over Siberia and Mongolia, deep Aleutian Low, and the Pacific subtropical ridge are a crucial setup for the CAO. It was found that the onset of the CAO is related to the breaking of atmospheric Rossby waves and vertical transport of vorticity that facilitates meridional advection. The study also indicates that intrinsic parameterization of the surface fluxes within the WRF model needs more evaluation and analysis.

Completed work – Summary

The completed work to date includes regional climate simulations (0.6° resolution) of the northern Pacific for the 1995-2010 period; high-resolution (0.1°) regional climate simulation of the Kuroshio current area; high resolution (0.1°) weather simulations of a cold air outbreak event 22-30 January 2000; analysis of the surface sensible and latent heat fluxes on high-resolution convection in the western Pacific; analysis of the sea surface temperature fields from satellite data, global climate models, and "normal year" ocean simulations (Large and Yeager, 2004); analysis of the flow fields over the western Pacific using global climate models and satellite data; and implementation of coupling mechanisms between the oceanic and atmospheric processes modeling.

Coupling of regional atmospheric (WRF) and ocean (POP) models to understand air-sea interaction in the western Pacific

One of the main objectives of this project was to develop a state-of-the-art Regional Ocean-Atmosphere Climate System Model to perform high-resolution simulations based on the well-developed Parallel Ocean Program *(*POP*)* as the ocean component and the Weather Research and Forecasting (WRF) model as an atmospheric component. Note that the POP model was mainly used as an ocean component of the global climate models (e.g., the Community Climate System Model (CCSM) and the Community Earth System Model (CESM)). However, in this study it has been used as a regional scale model to be coupled with WRF which has been already developed as a regional scale model. We believe that these efforts will facilitate focused regional studies to resolve the role of fine-scale critical details of the Pacific western boundary current (Kuroshio) and its effect on extratropical storm tracks by improved representation of feedbacks and local physical processes. Our initial attempts consisted of adapting the new CCSM flux coupling architecture CPL7 for our specific regional domains and model component configurations. CPL7 software was originally developed for coupling the global Community Atmospheric Model (CAM) and POP models (Fig. 1).

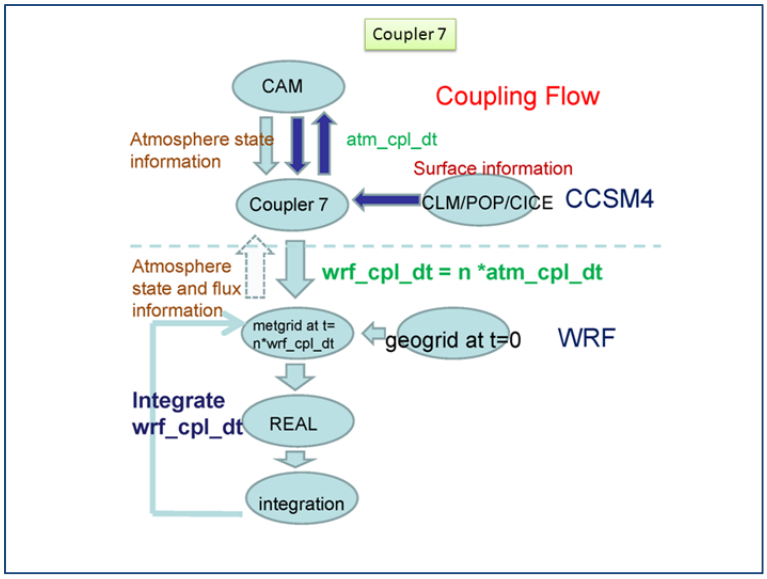

Figure 1: Schematic of the Coupler 7 system for global climate modeling.

This model framework has been adapted for different cases, e.g., the Regional Arctic Climate system Model (RACM). Using the same RACM system, we have attempted to separately configure WRF with prescribed ocean lateral boundaries (by the DRI team members) and POP with prescribed atmospheric lateral boundaries (by the SCRIPPS team members) as independent stand-alone model components (see domains in Fig. 2). After these steps, development of appropriate coupling schemes will then be adapted. Despite having direct, in-kind collaboration with model RACM developers, these efforts (initially performed in NERSC-Franklin) have suffered several difficulties that will be listed below. First, the model is available for public use but most of its integrated model components have not been tested for functionality and are still undergoing development and evaluations. As of today, only a couple of other similar but untested cases are available, some of which we are using to port and replicate in the newer NERSC-Hopper system. Secondly, most of the input data and grid configurations are not easily adaptable to special cases such as ours. All cases available use a separate Land Surface Model (LSM) component, the Community Land Model (CLM) version 3.5, which requires additional expertise for adaptation. We looked for guidance on adapting this component to our Ocean-Atmosphere configuration over the North Pacific with little success. The WRF-CLM configuration itself requires an additional grid configuration as well as an additional parameter for its setup. Both WRF and POP use different grid resolutions, projections, and domains which make the model setup difficult.

Alternatively, we started producing our own coupling configurations using RACM systems with POP as the ocean component running in a stand-alone format and WRF as the atmospheric components based on WRF "as is" (Fig. 3). For this, we created a coupling system that halts and synchronizes WRF and POP simulation times, exchanges information accordingly every coupling time step (~3 hours), and balances surface heat fluxes using the same domain configuration shown above (Fig. 1). These configurations provide easier coupling than RACM, since WRF configurations can be changed without affecting POP setup and other configurations. This coupler development handles all communications, performs interpolations between the different grids (several interpolation schemes will be implemented).

Additionally, this coupling strategy provides independence and flexibility between the codes, fully utilizes the developments from individual components (e.g., any WRF LSMs), and allows us to use the latest versions of the components (e.g., annual WRF updates).

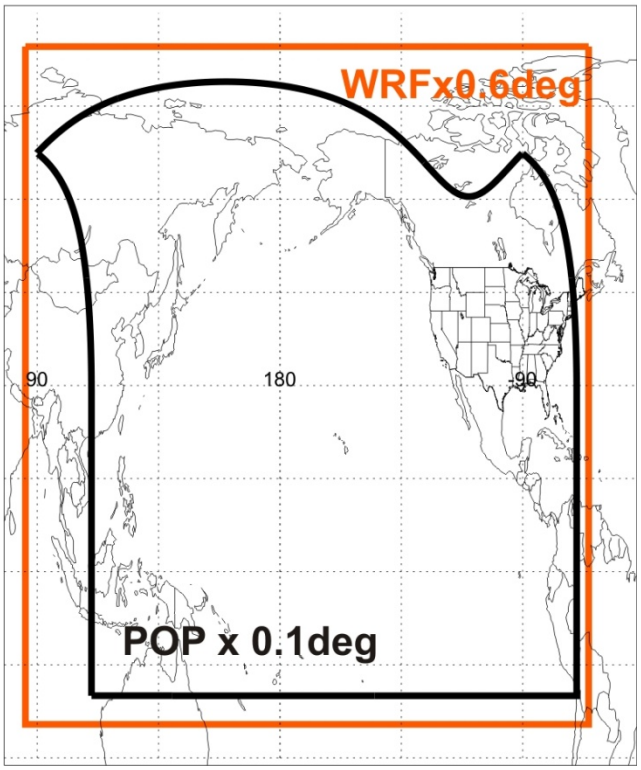

Figure 2: Regional POP and WRF domains for hindcast simulations. Both domains cover all of the North Pacific basin. Note the difference in domains, projections and grid size.

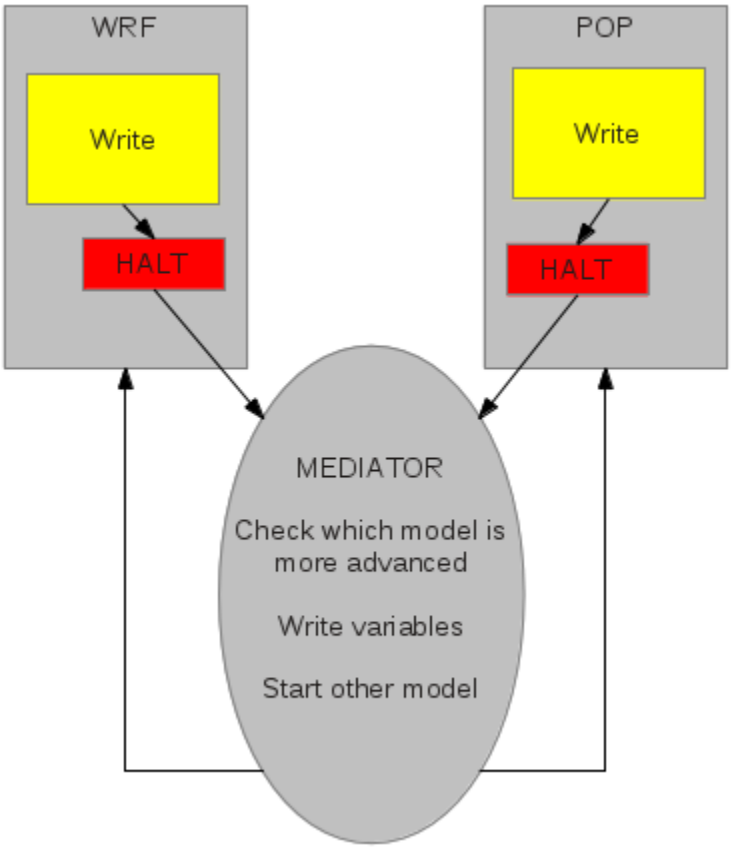

Figure 3: Schematic of the WRF and POP coupling system.

Status of the system

1) Mediator controls both POP and WRF
2) Optimizing the interpolation schemes
3) One-month test using WRF as stand-alone
4) One-month test using POP as stand-alone
5) One-month test fully coupled.

Air-sea interaction over the Kuroshio and Kuroshio Extension regions

It is well known that western oceans' boundary currents induce strong air-sea interactions. They represent the greatest mean and variability of the net surface heat flux over the oceans at multiple temporal scales (Wallace and Hobbs, 2006). One of the most intensive western boundary currents is the Kuroshio Current which flows along the south coast of Kyushu and Shikoku Islands, then separates from the Japanese coast and turns eastward as an inertial jet. This eastward jet is called the Kuroshio Extension (KE) and separates warmer subtropical water in the south from colder subpolar water in the north (Nonaka and Xie, 2004). Due to this separation, a sharp SST ocean front is formed with a significant change in the SST on the order of 10° C in 100 km. The current is dynamically unstable, which

causes the formation of large meanders and eddies (Mizuno and White, 1983) with the highest level of eddy kinetic energy in the Pacific Ocean (Wyrtki et al. 1976). The complexity of the current can be observed from satellite observations (Toba and Murakami, 1998).

Due to intense interaction of the atmospheric and oceanic processes, the Kuroshio region is one of the dominant areas with significant atmospheric convective processes. Figure 4 shows the annual surface net heat flux and the sea surface height in the North Pacific and indicates that the Kuroshio area is a heat source that overwhelmingly contributes to the weather and climate of the North Pacific. The impact of the Kuroshio-forced induced heat transfer is further enhanced in the winter by stochastic cold air outbreaks (CAOs) from Eurasia. They occur approximately 13 times during a usual synoptic setup of the Siberian-Mongolian High and the Alaskan Low during boreal winter (Dorman et al. 2004). Most of the time, cold stable air accumulates over inland Russia, China, and Mongolia due to large scale surface energy loss due to radiational cooling of snow covered land and clear sky conditions under the Siberian anticyclone as well as advection from colder polar latitudes to the north. This cold inland airmass is effectively blocked by coastal mountains and contained within the continental margins. However, mountain gaps, for example a gap approximately 150km wide and located north of Vladivostok offers a passage for the trapped airmass to escape into the Sea of Japan and eventually over the open western Pacific and Kuroshio region. On an average of 3-5 times during January and February, a perturbation of this synoptic setup occurs and allows an intrusion of very cold air to flow through the mountain gaps, over the coastal mountains, or a combination of the two. The intruding air is usually 15^{o}C (or greater) colder than the underlying ocean sea surface, generating a severely convectively unstable environment that is conducive to mixing and subsequent upward heat transfer from the surface. The main objective of this component of the collaborative study with Scripps was to understand the impact of the Kuroshio currents on the atmospheric dynamics and thermodynamics.

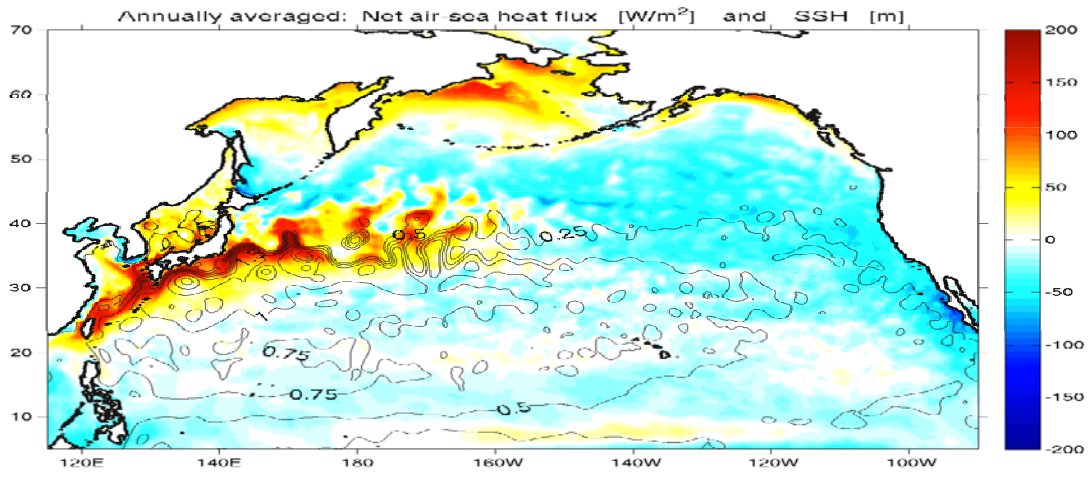

Figure 4: Annually-averaged net air-sea surface flux (W m^{-2}) and the sea surface height (m) in the Northern Pacific.

Model setup for weather and climate modeling

The horizontal domain of the atmospheric model was configured in a nested mode, with the parent domain covering the entire North Pacific Ocean Basin on a cylindrical equidistant latitude-longitude projection and an innermost domain focusing on the Japan Sea and the Kuroshio and Kuroshio Extension (KE) regions.

Figure 5: The WRF model domains for regional climate and weather simulations.

Since the observational network over this vast region is quite sparse and our goal is to understand the roles and interactions of all the relevant processes, we simulated this event using the WRF model. There were two model domains (Figure 5), the coarse, outer domain used a 0.6^{o} resolution and the nested inner domain used a 0.1^{o} resolution. The model was run from 22 January at 00 UTC to 28 January 2000 at 00 UTC using Global Forecast System Final Analysis (GFS-FNL) data for the initial and boundary atmospheric conditions. The main setup parameters were:

Model domain configuration:

Parent domain: horizontal grid resolution: 0.6° (325 × 159 grid points)
Horizontal grid configuration = lat-lon
Number of vertical levels = 33
Domain coverage = [25^{o}S – 70^{o}N; 100°E – 65°W]

Nested domain: horizontal grid resolution: 0.1° (601 × 451 grid points)
Number of vertical levels = 33
Domain coverage = [15°N – 60°N; 120°E – 180°E]
Physics: Mellor-Yamada-Janjic boundary layer scheme
Kain-Fritsch cumulus scheme
Morrison double moment microphysics scheme
Radiation: Rapid Radiative Transfer Model (RRTM)

A component of this project was to develop a coupled atmosphere-ocean model on a regional scale using the WRF atmospheric model and POP ocean model to perform high resolution (~10km or 0.1^{o} grid size) simulations. These efforts will facilitate focused regional studies to resolve the role of fine-scale critical details of the Pacific western boundary current physics and their impact on the atmosphere. The study will also reveal the effects of these intense sea-air interactions on extratropical storm tracks. Initial and boundary conditions for the WRF climate simulations were created by CCSM3. For the high-resolution weather modeling on the same domain, we used GFS-FNL initial and boundary conditions from NCEP.

Cold air outbreak event 22-27 January 2000

Figure 6 shows the main study area with selected buoy (21002 and 21004) and radiosonde (Vladivostok and Hachijyojima) locations. Vladivostok is located near a coastal mountain gap (approx. 150 km wide) where most of the intrusion starts during the CAOs, buoy 21002 is in the southeast part of the Japan Sea, and Hachijyojima and buoy 21004 are representative of the western edge of the KE region.

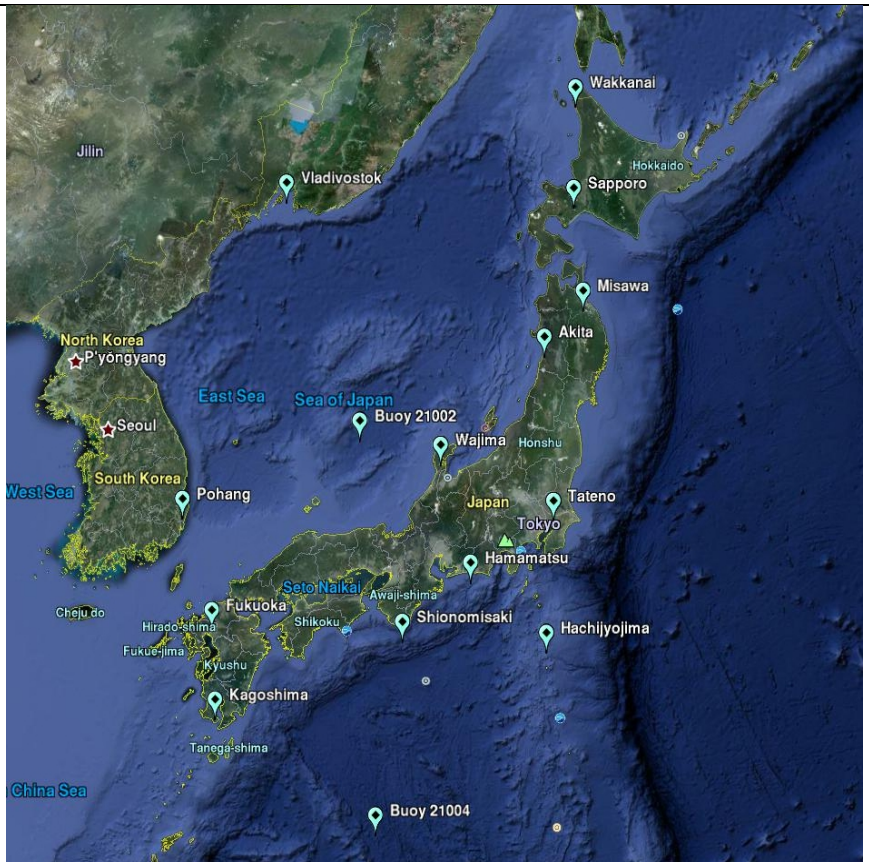

Figure 6: Study area in the western Pacific with indicated buoy and radiosonde measurement locations.

Figure 7 shows radiosonde measurements of the air temperatures and calculated potential temperature at Vladivostok and Hachijyojima from 22 to 27 January 2000. There was a significant cooling within the

first 5 km during this event at Vladivostok with a deep stable layer extending to about 10 km. At Hachijyojima there was warming present from the surface until about 6 km and cooling aloft with the generation of multiple convectively unstable layers.

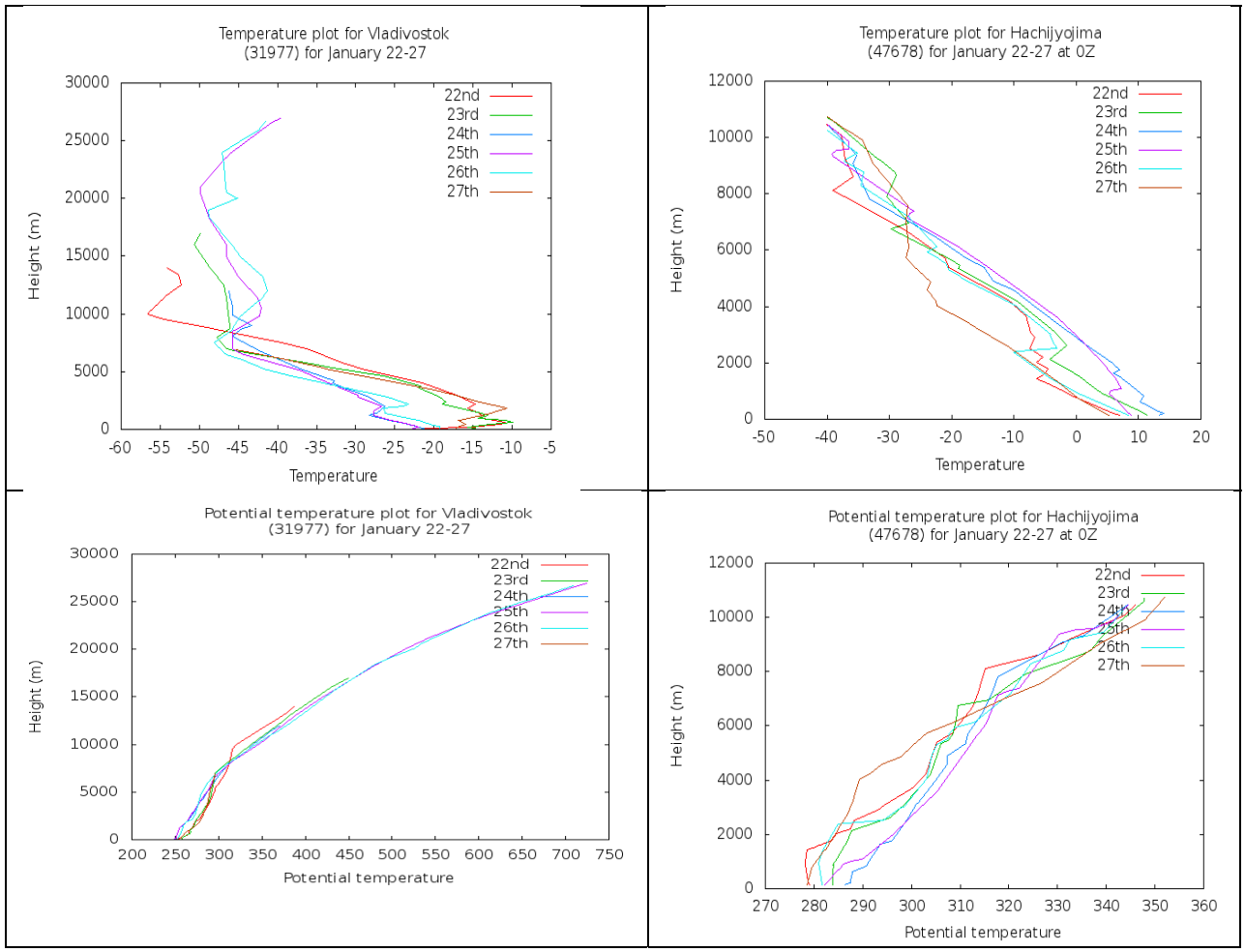

Figure 7: Radiosonde measurements of the evolution of the air (upper panels) and potential (lower panels) temperatures at Vladivostok (left column) and Hachijyojima (right column) from 22 to 27 January 2000. Notice that the vertical scale is different since the Hachijyojima soundings extend only to 12 km while Vladivostok measurements are up to 30 km.

It is well accepted that over eastern Asian and the western Pacific a portion of the largest amplitude stationary wave on the globe exists (Wallace, 1983) as a result of the synoptic centers of the Siberian and Mongolian anticyclone with the Aleutian Low to the east, and the subtropical ridge to the south. It is of interest to examine the stability of this synoptic setup and possible relationships between the stability of the wave and the onset of CAO events. The current research demonstrates that the CAO is an example product of the behavior of coupled nonlinear multiscale phenomena encompassing the atmospheric, land surface, and oceanic components of the Earth system. Preliminary results highlight the importance of extremely high-resolution numerical modeling and observational networks to capture the key processes. An examination of the re-analysis fields indicates that the CAO was preceded by a anticyclonic Rossby wave break and intrusion of high isentropic potential vorticity air into the midlatitudes.

Model evaluation and surface fluxes

We performed model evaluation of atmospheric vertical profiles at two radiosonde sites. The first site, Vladivostok, Russia, is in the area of a strong anticyclone and south of a coastal mountain gap of about 150 km wide where one part of the CAO originates (Fig. 6). The other site, Hachijyojima, is on an island just west of Japan in the Kuroshio area. Figure 8 shows a comparison of the wind speed and direction between the WRF and the radiosonde observations at Vladivostok and evidences that the WRF model accurately represented the dynamics through the whole period. There was a deep (~6 km with speeds greater than 40 m s^{-1}) and strong jet with the maximum speed reaching 50 m s^{-1} at about 8 km. During the 5-day period the winds were entirely from the NW quadrant throughout the entire vertical range of 18 km. In the beginning of the period (22 January), the near-surface winds were weak and southwesterly under the influence of the subtropical ridge. The CAO started the next day as indicated by an increase in wind speeds and directional shift to northerly and northwesterly. Cold air advection can be observed by the backing pattern of winds (counter-clockwise rotation with height) The subtropical ridge retreated eastward and the Siberian anticyclone extended southward. The near-surface wind velocities stayed high during the CAO event. Although a part of the model's success lies in the fact that the initial and lateral boundary conditions from the re-analysis which assimilates twice-daily radiosonde observations, it still shows that the evolution of the process and magnitude of the basic parameters were well captured.

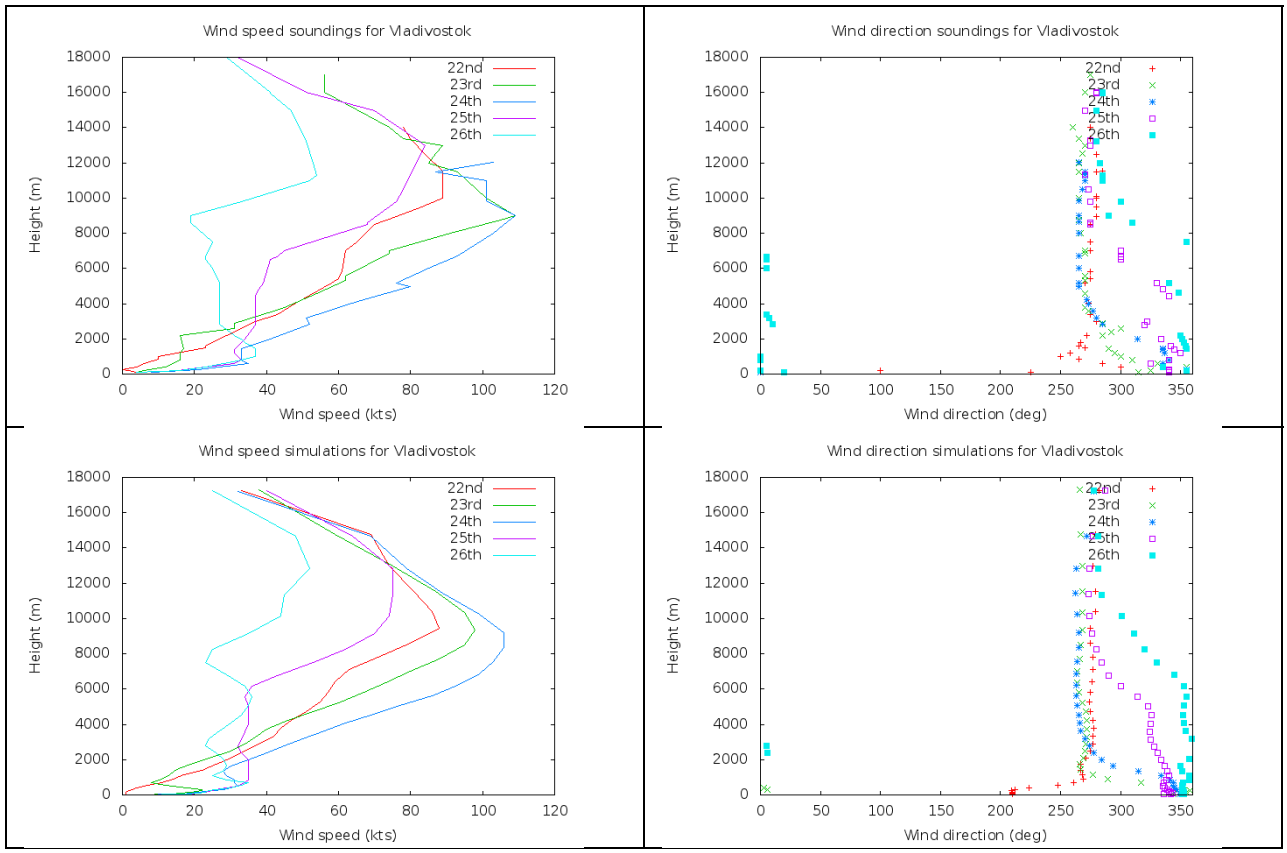

Figure 8: Comparison of the observed (upper panels) and modeled (lower panels) wind speed (left panels) and wind direction (right panels) at Vladivostok from 22 through 27 January 2000.

The model also showed fairly good agreement with buoy data. Figure 9 shows time series of the measured and simulated air and sea surface temperature (SST) at buoys 21002 and 21004. The cold air outbreak started around 24 January at buoy 21002 (Japan Sea) and a day later at the buoy 21004 (KE region). Notice that the SST was between 12°C and 13°C in the SE Japan Sea, while the SST over the KE region was between 20°C and 21°C. In spite of this contrast, the air-sea temperature difference and consequent surface heat fluxes in the period considered were greater over the Japan Sea, reaching 15°C, while over the KE region the differences were less than 10°C.

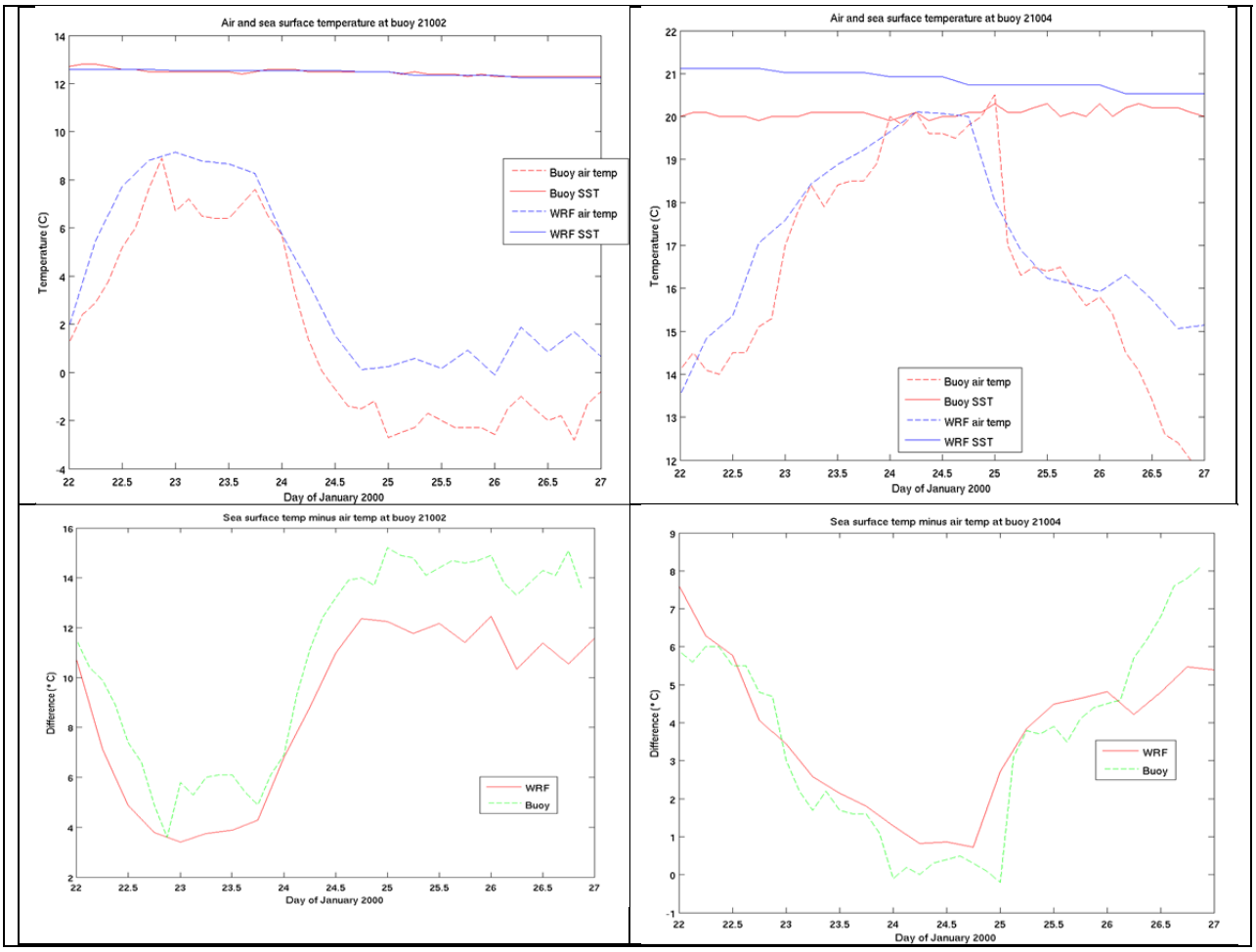

Figure 9: Time series of the air and sea temperatures (upper row) at buoys 21002 (left column) and 21004 (right column). The bottom row shows differences between the sea and air temperatures. WRF (buoy) SST is shown with solid blue (red) line, WRF (buoy) air temperature with dashed blue (red) line. WRF (buoy) differences between the sea and air temperatures are shown in red (dashed green) during 22-28 January 2000.

Although the model was able to reproduce buoy temperatures well (Figure 9), the intrinsic model-computed fluxes are underestimated compared to the fluxes calculated using the bulk formulae (Figure 10).

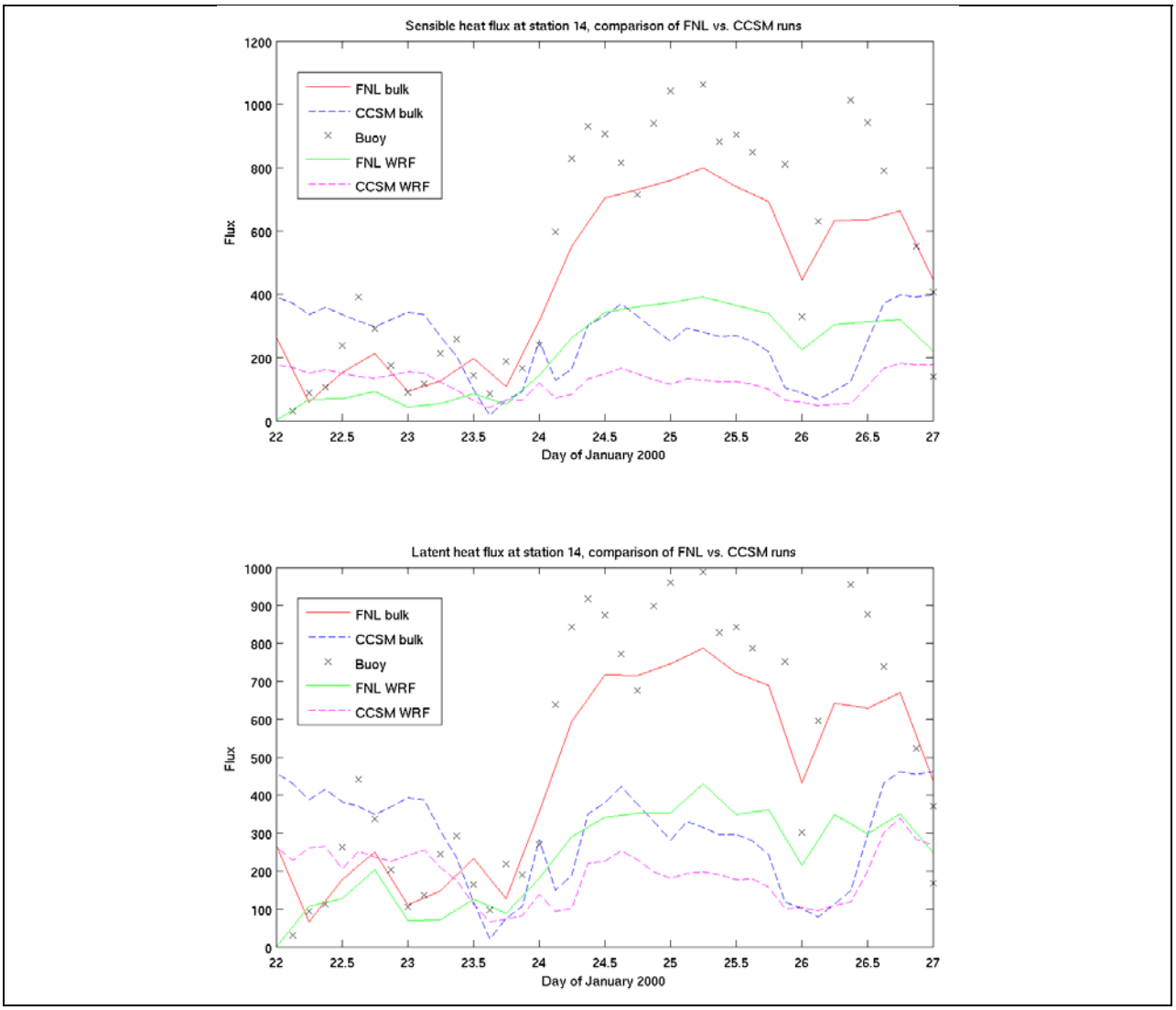

Figure 10: Sensible and latent heat fluxes at buoy 21002 as computed from measurements (x), simulated by WRF with FNL inputs (green) and CCSM inputs (dashed magenta), and computed by bulk formulae using WRF main parameters as input (red; dashed blue).

Over the Japan Sea, the buoy-calculated sensible fluxes were in excess of 1000 W m^{-2}, while the model parameterizations yielded a maximum of 400 W m^{-2}. Buoy latent heat fluxes approached 1000 W m^{-2} while the modeled fluxes again reached a maximum of 400 W m^{-2}. To understand these differences better, we also used modeled temperatures and moisture to compute the values using bulk formulae (red lines in the figure). This provided significant improvement, especially for the sensible heat flux at buoy 21002. Although bulk formulae have assumptions and approximations, for example the heat transfer coefficient varies with wind velocity and temperature, they still indicate that for these types of temperature and moisture differences, the fluxes should be of greater magnitude than determined by WRF. The results from the bulk formulae suggest a thorough evaluation of the surface flux parameterizations in the model is necessary, particular for improving regional climate simulations. The surface fluxes computed from observations and simulations are shown in Figure 11.

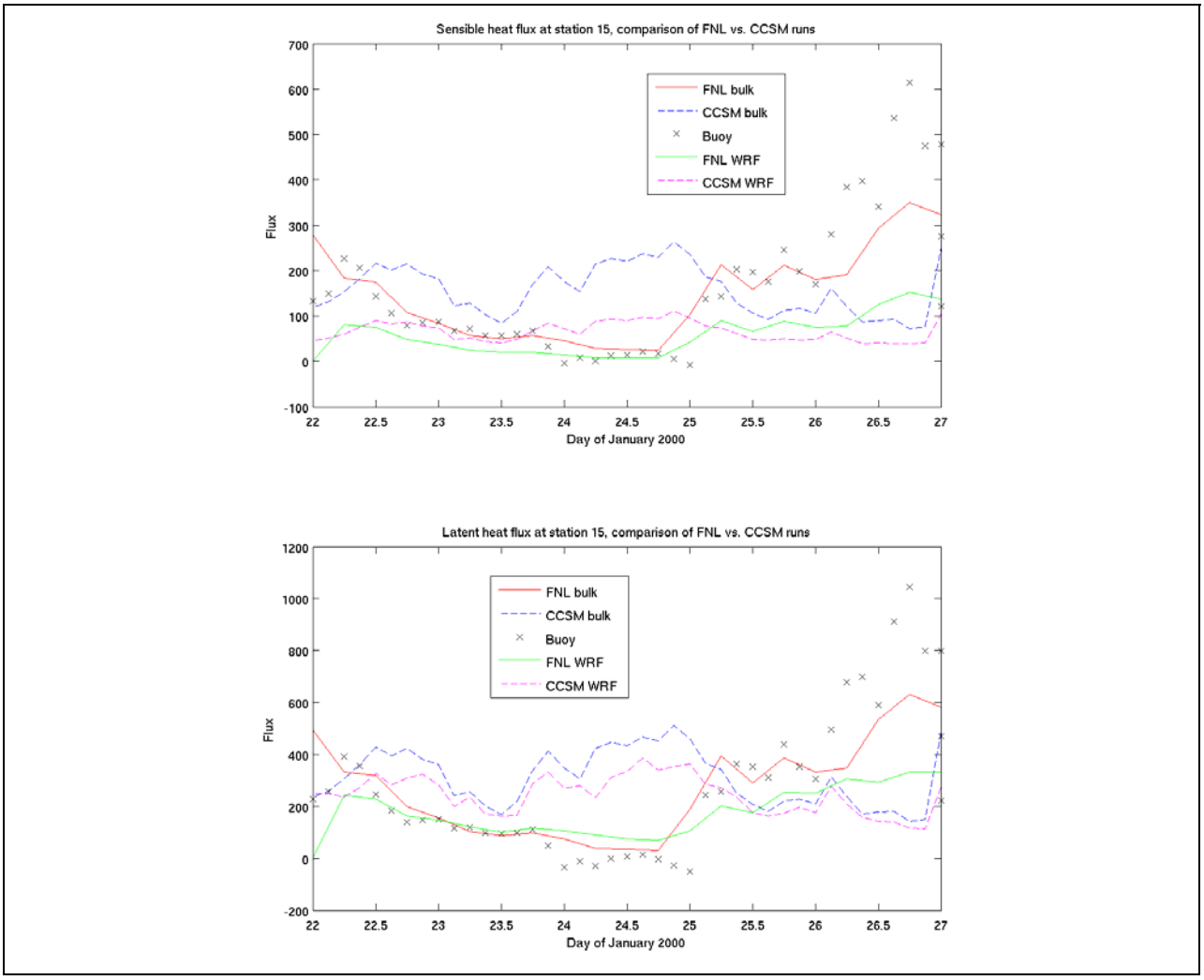

Figure 11. Sensible and latent heat fluxes at buoy 21004 as computed from measurements (x), simulated by WRF with FNL inputs (green) and CCSM inputs (dashed magenta), and computed by bulk formulae using WRF main parameters as input (red; dashed blue).

Problems are apparent with the simulated fluxes at both buoy locations. The implicit WRF schemes significantly underestimate the fluxes. As a test, we used the simple bulk formulae with temperature, humidity and winds as inputs from the WRF outputs. As shown in Figures 10 and 11, the application of the bulk formulae provided a significant improvement. Consequently, there is a need to further evaluate the WRF surface flux parameterization schemes for these strong convective conditions and understand reasons for discrepancies.

Synoptic setup and formation of transient mesoscyclones

Prior to the event, a synoptic setup was characterized by the Siberian-Mongolian High (SMH) with the pressure in excess of 1060 hPa in the center, the Aleutian Low (AL) with the pressure lower than 975 hPa in the center, and the subtropical ridge extending over the Japanese islands and inducing a

southwesterly flow over the Japan Sea and the Kuroshio Extension (KE) area. The pressure gradients between the SMH and AL generate favorable conditions for onset of the CAO. The SMH air is stably stratified and generally blocked by the Asian coastal mountain ranges. During certain atmospheric conditions, the pressure gradient intensifies and the SMH flow intrudes through the mountain gaps and over the mountain tops. The intrusion starts on the northern side where the gradients are greatest and extends to the south through the Vladivostok gap and over the coastal mountains. Dominant southwesterly flow over the Japan Sea retreats to the south due to encroachment of the stronger northerly and northwesterly flows from the eastern edge of the SMH, which intensifies and extends over the islands of Japan and the KE region. This interaction forms flow convergence zones that extends to the southeast. The northerly and northwesterly flow over the Japan Sea becomes blocked and channeled by the Korean Peninsula's coastal mountains and attains a cyclonic rotation near the gap between the southern tip of Korea and Japan. During this event, the rotation resulted in formation of transient mesocyclones which travel from the southern side of the Japan Sea eastward over Japan and the KE region. Additional convergence is generated due to the interaction of the outbreak advection (north and northwesterly) with the southwesterly flow from the subtropical ridge in the southern Pacific. Consequently, there are two mechanisms at work during the CAO – the straightforward northerly and northwesterly advection of cold continental air and then additional southwesterly and westerly transport by poleward mesocyclones. In order to evaluate the appearance of the simulated mesocyclones, we examined QuikSCAT wind fields that can indicate possible convergence zones and formation and evolution of the transient mesoscyclones. Figures 12 and 13 show snapshots of the QuikSCAT derived-and simulated wind fields at corresponding times.

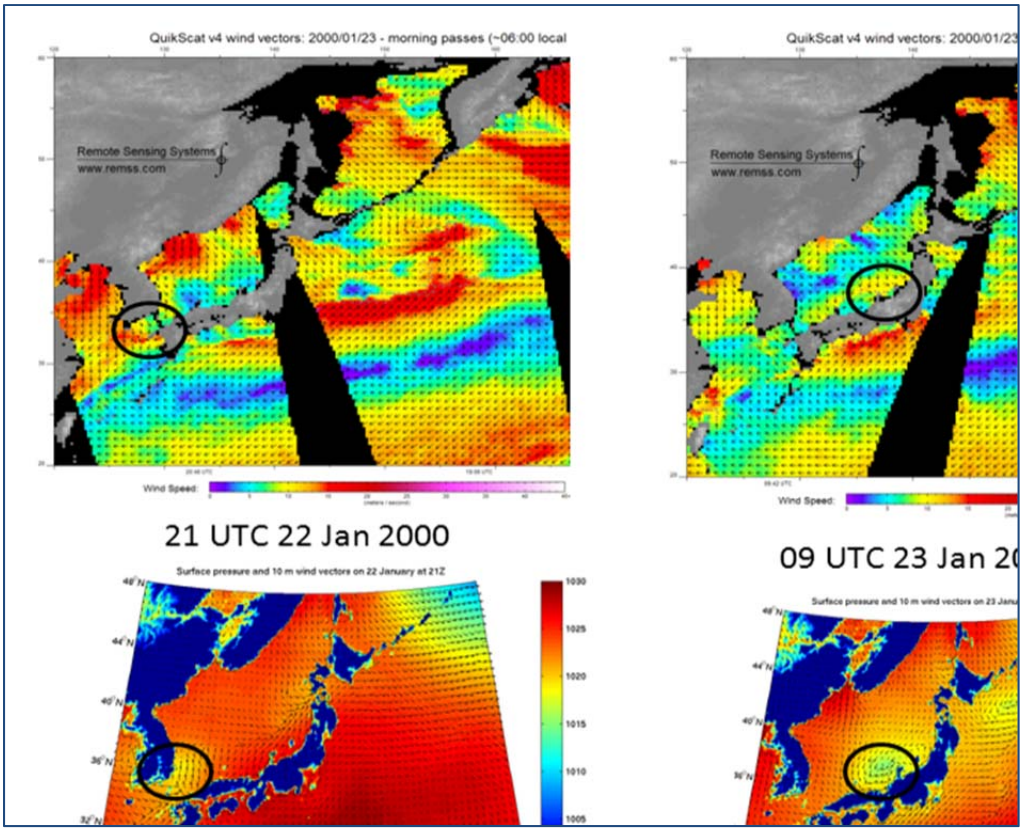

Figure 12: Snapshots of the vector winds from QuikSCAT (top row) and WRF simulations (bottom row).

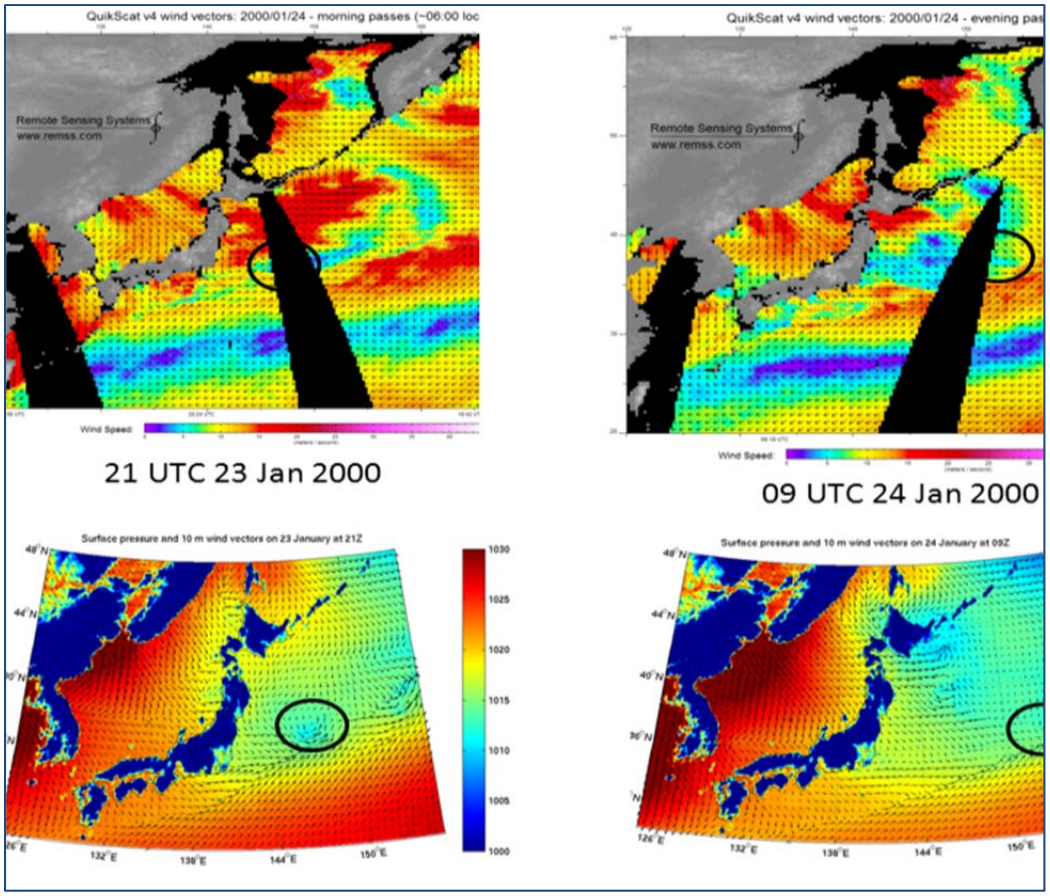

Figure 13: Snapshots of the vector winds from QuikSCAT (top row) and WRF simulations (bottom row).

Meso-lows moving rapidly across the area on an easterly track are the key to the quickly changing surface atmosphere of the Japan Sea and the northwestern Pacific. The figures are shown at four times for the period of 21 UTC 22 Jan 2000 to 09 UTC 24 Jan 2000. The lower panels are WRF simulations of wind vectors and sea level pressure. The upper panels are QuikSCAT data from http://www.ssmi.com/, with direction plotted as wind vectors and speed represented as color and data/time matching the WRF panel below. This series starts with a meso-low center (under the circle) between Korea and Japan (21 UTC 21 Jan), that moves across the southern side of the Japan Sea (09 UTC 22 Jan), crossing over to the east of Japan (21 UTC 23 Jan), then moving further east (09 UTC 24 Jan). The meso-low moving across Japan and toward the east instigated an additional mechanism (besides the straightforward northerly and northwesterly advection over the coastal mountains) for enhancing the very cold Siberian air outbreak, pushing across the Japan Sea to the Pacific on 24 Jan.

The findings from the analysis and simulations of the enhancement of the CAO by transient meso cyclones are being elaborated on in a manuscript in preparation (Koracin et al., 2013).

Midtropospheric Response to a Siberian Cold Air Outbreak

The NCEP/NCAR Reanalysis 2.5° - resolution dataset (Kalnay et al., 1996) was used to compare anomalous atmospheric conditions preceding a severe Siberian cold air outbreak that began on January 23, 2000. Climatological means (based on 1980-2011 data, only satellite-era measurements and post-PDO shift climatology (mid-1970s) were desired to be included for this analysis) and anomalies were derived for the time period of January 18-22, 2000 for several levels in the atmosphere (1000 mb, 500 mb, 300 mb). Figure 14 demonstrates the climatological means while Figure 15 presents the anomaly fields. Note that while many fields are used in both cases, several anomalies are presented without corresponding mean fields. The following descriptions will begin from the surface, or lowest level, and continue upwards through the atmosphere.

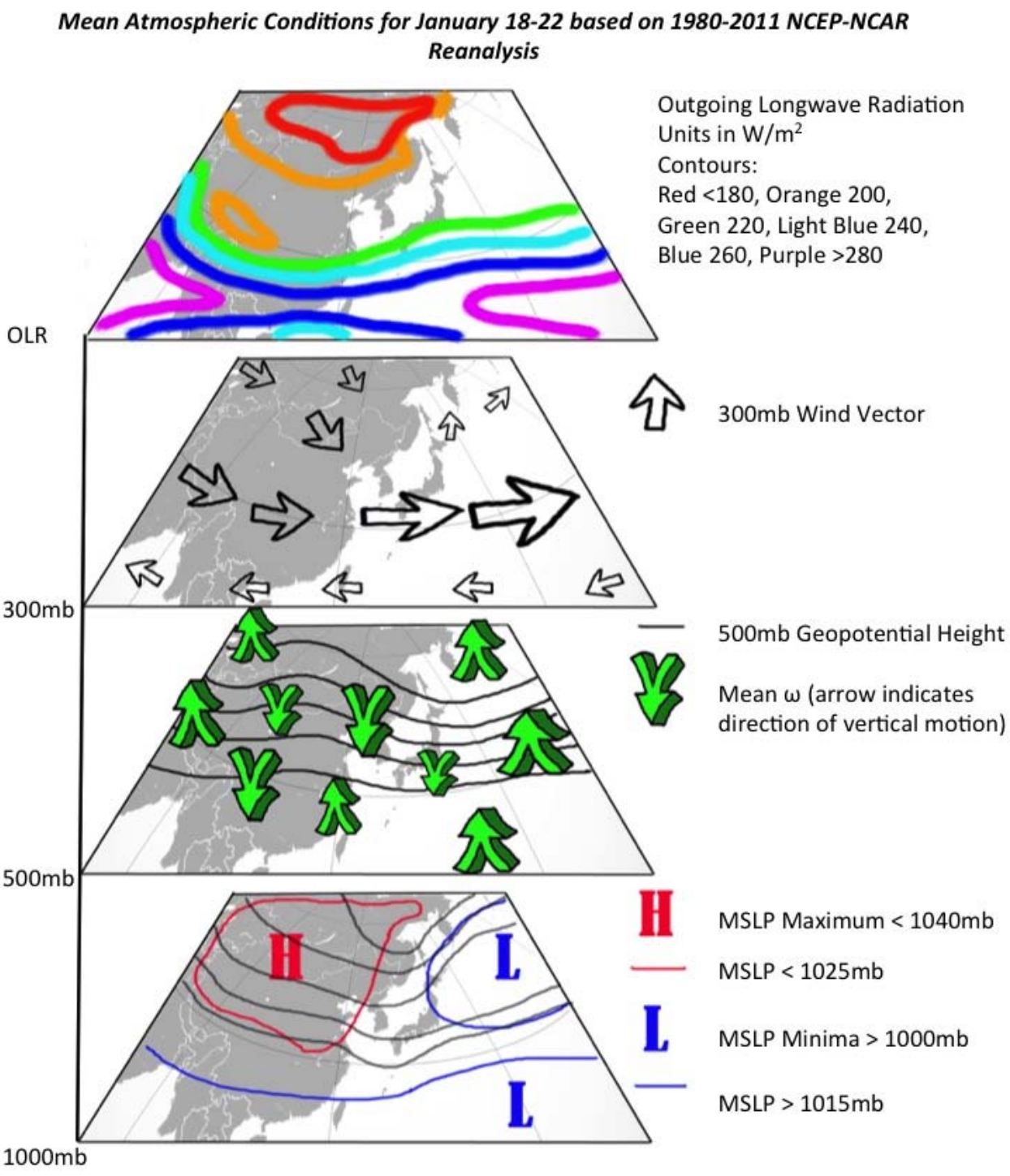

Figure 14: Mean atmospheric conditions (1980-2011) for the study domain.

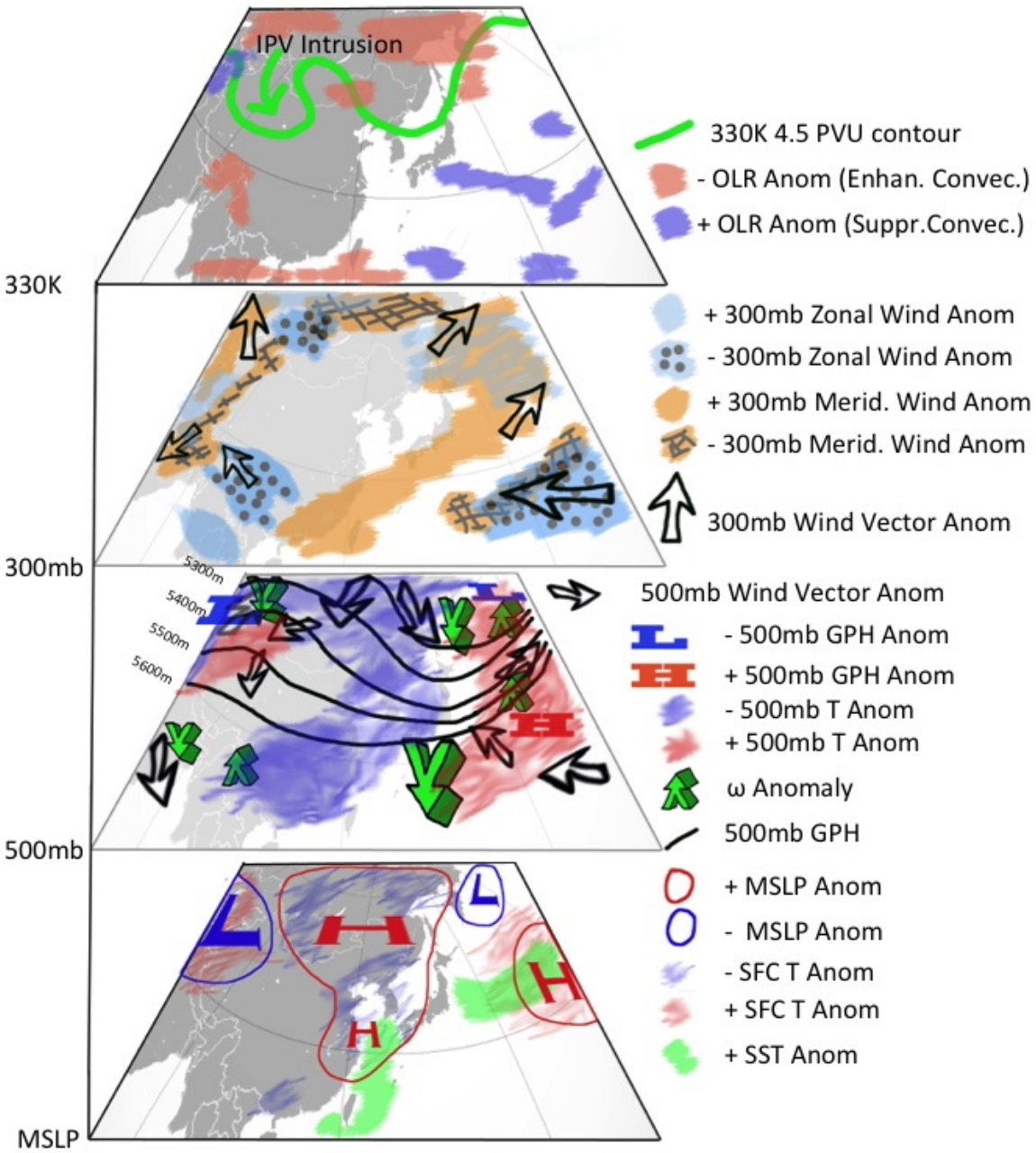

Figure 15: Anomalous conditions during the CAO event (18-22 January 2000).

Mean sea level pressure fields corresponding to persistent low (high) pressure less than 1015 mb (greater than 1025 mb) are indicated in Figure 14 by blue (red) lines. The mean location of the Siberian-Mongolian High (1045 mb) is indicated by the *red H* while the mean locations of the Aleutian Low to the

north and ITCZ-induced tropical low to the south are shown by the *blue L's*. Surface air temperature isotherms are designated by the black contour lines and correspond to temperatures of 275 K (southern line) to 250 K (northern line) with a contour interval of 5 K. The lowest mean temperatures do not correspond directly to the location of the Siberian High due to the longer duration of seasonal snow and ice cover as well as the lower solar net radiation in the northern most latitudes. A significant temperature gradient exists to the south of Japan and along the northern Asian coastline due to the moderating influence of the relative warmer ocean waters which are heated by the Kuroshio western boundary current transporting tropical waters warmed by strong solar radiation towards the poles. Ephemeral sea ice in the marginal Sea of Okhotsk during boreal winter causes lower temperatures to extend beyond the continent and over the ocean.

The second panel from the bottom highlights the 500 mb geopotential heights (black contour lines) and associated vertical motion (green arrows) as inferred from the quasigeostrophic omega equation. The persistent ridging associated with the Siberian-Mongolian High is clearly evident over southern Siberian and northern Mongolia while a persistent trough is located over the East China Sea. A strong planetary-scale temperature gradient is formed between the relatively warm tropical western Pacific and the relatively cold Asian continent while the upper tropospheric low pressure over Siberia and high pressure over the western Pacific generates a favorable baroclinic environment to form a merged polar and subtropical jet (East Asian Jet, EAJ). The divergent exit region of the EAJ and associated upward vertical motion is shown by the strong negative ω to the east of Japan. Other locations of persistent negative ω are found over the western tropical Pacific, upstream of the Siberian High in a persistent low formed over the Caucasus, in the region of the Aleutian Low, and near the coast of southern China, likely due to the variability of the EAJ exit region location. Climatological areas of subsidence, or positive ω, are found over the core Siberian High region and in the convergent entrance region of the EAJ.

The 300 mb wind vectors are demonstrated in the third panel from the bottom. The arrow size is proportional to the velocity. The tropical easterlies are well defined as is the high eastward velocity resulting from the EAJ. Northwesterly flow deriving from the anticyclonic Siberian High is present over northern Asia while southerly flow exists over the Bering Sea. Finally, the top panel shows the mean outgoing longwave radiation (OLR) that can be used to infer the presence of cloud cover due to convective processes or surface temperatures in the absence of clouds. In accordance with the surface snow and ice cover in the northern extents of Asia, very low values of OLR are observed. In the tropical areas, the presence convective clouds generate relatively low OLR values, as these clouds radiate at their cloud top temperature. These temperatures tend to be low as the tropical atmosphere is in a state of radiative convective equilibrium and the cloud tops penetrate high into the troposphere. The subtropics demonstrate higher values of mean OLR, however a tight gradient exists during boreal winter as the probability of continental snow cover increases with latitude thus reducing mean OLR.

We now move to the anomalous conditions shown in Figure 15. Again starting at the surface, we see an enhanced Siberian-Mongolian High and subtropical ridge and correspondingly enhanced Caucasus and Aleutian Lows. The blue (red) contours indicate anomalous low (high) mean sea level pressures while the L (H) indicates the location of the center of the anomalies. Associated with these mean sea level pressure anomalies we observe warm surface air temperature anomalies in the Kuroshio and Caucasus

regions and anomalously cold surface air temperature anomalies in Siberia, Mongolia, and eastern mainland China and Manchuria. The green shading demonstrates warm sea surface temperature anomalies in the southern Sea of Japan and western central Pacific, perhaps due to enhanced transport by the Kuroshio and Kuroshio extension currents.

The surface tendencies are explained further by 500 mb anomalies shown in the second panel from the bottom. An amplified Rossby wave pattern over Asia exists with anomalously high geopotential heights (black contour lines) and surface pressures (H and L, for clarity these are also shown in the 500mb panel) over Siberia and in the central Pacific and anomalously low geopotential heights over the Caucasus and Japan. Blue (red) shading indicates anomalously cold (warm) 500 mb temperatures. The cold anomalies are located downstream of the Siberian High while warm anomalies are observed over the Caucasus and western Pacific. The enhanced temperature gradient appears to be driving the amplified planetary wave pattern via the hypsometric equation. Black arrows show the 500 mb wind vector anomalies which appear to highlight enhanced equatorward flow from the high latitudes and an acceleration of westerly flow east of Japan due to the divergent exit region of the curved 500 mb jet. The green arrows (ω) provide further evidence for the enhanced divergence and upward vertical motion associated with the 500 mb jet exit region and subsiding motions due to the enhanced ridge corresponding to the Siberian High.

Moving upward to 300 mb, the third panel from the bottom demonstrates changes in jet stream level meridional winds with blue shading (dotted blue) corresponding to increased (decreased) winds. Zonal wind anomalies are shown with orange shading (striped orange) corresponding to increased (decreased) winds. The black arrows are used to show vector wind anomalies. Anomalous increases in both zonal and meridional winds are apparent over the northern west Pacific while to the west of the amplified Siberian high, anomalous decreases in zonal and meridional winds are observed. Strong decreases in both are also observed in the region of the EAJ and demonstrate a westward retraction of the EAJ. Zonal 300 mb winds are enhanced all along the coast of Asia.

The fourth panel presents the negative OLR anomalies in salmon (purple) and a contour of isentropic potential vorticity (IPV) 4.5 PVU (potential vorticity units, m2 s-1 K kg-1) contour in green; this field is calculated from NCEP-NCAR Reanalysis data using Ertel's form of the potential vorticity equation. A deep intrusion of high IPV air from the polar vortex is evident and demonstrates the process of an anticyclonic IPV wave break. Evidence of enhanced convection over the Indian Ocean and Maritime Continent is observed while there is reduced cloud cover over the Kuroshio extension region east of Japan.

The NOAA Climate Prediction Center's El Nino-Southern Oscillation (ENSO) index and Pacific-North American (PNA) index indicated conditions of a strong La Nina and weak positive phase of the PNA (not shown). However, the observed anomalous conditions are in agreement with the state of both of these large scale features. An amplified (blocking) Rossby wave pattern has been established over Asia and the Pacific thereby increasing the likelihood of polar CAOs and favoring an eastward extension of the EAJ. Tropical convection is enhanced over the Maritime continent, consistent with La Nina conditions. A switch from a negative phase of the PNA to a positive phase during December may explain the current retraction of the EAJ. The system appears to behave as a harmonic oscillator that, prior to the outbreak,

has contracted and maximized its potential energy. The triggering mechanism is the equatorward intrusion of high IPV air from the polar vortex which forces the amplified blocking Rossby wave pattern over Siberia to break, sending high IPV air into the midlatitudes. The associated trough thinning helps to force polar air south and begin the CAO. Anomalously warm sea surface temperatures resulting from an enhanced Kuroshio flow transport regime offer a prime environment for the subsequent air-sea interactions and diabatic forcing that will eventually result in the eastward extension of the EAJ over the Pacific, consistent with the positive phase of the PNA.

The findings from the analysis and simulations of the midtropospheric response to a Siberian Cold Air Outbreak are being elaborated on in a manuscript in preparation (Hatchett et al., 2013).

References

Dorman, C. E., R. C. Beardsley, N. A. Dashko, C. A. Friehe, D. Khelif, K. Cho, R. Limeburner, and S. M. Varlamov, 2004: Winter marine atmospheric conditions over the Japan Sea. J. Geophys. Res., **109**, C12011, doi:10.1029/2001JC001197.

Hatchett, B., C. Dorman, M. Kaplan, D. Koracin, T. McCord, and J. Mejia, 2013: Anatomy of a Siberian Cold Air Outbreak Part I: Triggering mechanisms and subsequent air-sea Interactions. (In preparation).

Kalnay et al., 1996: The NCEP/NCAR 40-year reanalysis project, Bull. Amer. Meteor. Soc., **77**, 437-470.

Koracin, D., C. Dorman, J. Mejia, B. Hatchett, I. Cerovecki, R. Vellore, and T. McCord, 2013: Air-sea interaction over the Kuroshio current during a cold-air outbreak. (In preparation).

Large, W., and S. Yeager, 2004: Diurnal to decadal global forcing for ocean and sea-ice models: the data sets and flux climatologies. NCAR Technical Note: NCAR/TN-460+STR. CGD Division of the National Center for Atmospheric Research.

Mizuno, Keisuke, Warren B. White, 1983: Annual and interannual variability in the Kuroshio Current system. J. Phys. Oceanogr., 13, 1847–1867.

Nonaka, M., and S.-P. Xie, 2003: Co-variations of sea surface temperature and wind over the Kuroshio and its extension: Evidence for ocean-to-atmospheric feedback. J. Climate, 16, 1404–1413.

Toba, Y. and H. Murakami, 1998: Unusual behavior of the Kuroshio Current system from winter 1996 to summer 1997 revealed by ADEOS-OCTS and other data—Suggestion of topographically forced alternating-jet instability. J. Oceanography, 54, 465-478

Wallace, J. M. (1983), The climatological mean stationary waves: Observational evidence, in *Large-Scale Dynamical Processes in the Atmosphere*, edited by B. Hoskins and R. Pearce, pp. 27–54, Academic, San Diego, CA.

Wallace, J.M., P.V. Hobbs, 2006: *Atmospheric Science*. Academic Press, pp 504.

Wyrtki, K., L. Magaard and J. Hager,1976: Eddy energy in the Oceans. J. Geophys. Res., 81, 2641–264.